10 Component-Minimized Three-Phase Power Converters

10.1 SOLUTIONS FOR REDUCTION OF NUMBER OF COMPONENTS

Previous chapters have extensively analyzed the three-phase converter based on six power semiconductor switches. One of the major preoccupations for the use of this conventional topology within industrial products is related to cost reduction. It has been shown that the largest cost share corresponds to building the power stage. Accordingly, one approach to cost reduction would rely on seeking new topologies with a reduced number of components. This is especially important for applications in the horsepower range up to several tens of kilowatts.

Different solutions have been reported in the literature during the last twenty years or so. An important research direction has been dedicated to new grid interfaces with power factor correction. Some of them, including the single-switch, three-phase AC/DC converter, were analyzed in Chapter 9.

Constraints of variable frequency and magnitude for AC motor-drive applications have limited the efforts for new power converters used for simplified three-phase AC sources. All reported solutions combine advantages and disadvantages versus the conventional six-switch inverter and none of them has really captured the market. These new solutions different from the conventional six-switch converter must be understood and studied for their merits and for the opportunity they provide to open up new directions for further research. They can be grouped in two categories:

- New inverter topologies: with reduced component count.
- Direct converters: to employ a single-power stage without intermediate DC link capacitor to perform direct AC/AC conversion.

10.1.1 New Inverter Topologies

The most well-known topology with reduced component count is shown in Figure 10.1 [1–12]. It is based on two inverter legs while the third phase is taken from the DC capacitor midpoint. This topology has proven merit to be considered for industry implementation. For this reason, a special part of this chapter is

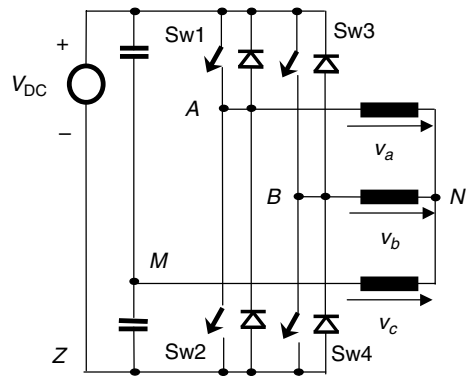

FIGURE 10.1 Topology for a B4 inverter.

dedicated to its full analysis. Similar application to AC/DC conversion stages has been considered.

An interesting combination of this topology, with a single-phase front-end converter, enabled use of a six-pack module for implementation of the whole AC/DC/AC conversion (Figure 10.2) [13]. The drawback is in the larger value of the DC capacitor bank. The two conversion stages (AC/DC and DC/AC) are controlled totally independently and the additional control module manages the DC voltage within two threshold levels. A quick comparison with conventional topologies outlines the larger DC voltage on the bus. This aspect will be detailed in Section 10.2 and Section 10.3.

A completely different approach to reducing the number of components in the AC/DC/AC power electronic conversion supports a unidirectional load current (Figure 10.3a) [14–17]. If the load is a three-phase AC machine, it can be proven that this DC component does not affect the torque production but only increases the machine losses. Each leg is reduced to a DC/DC converter with a variable reference, as shown in Figure 10.3b.

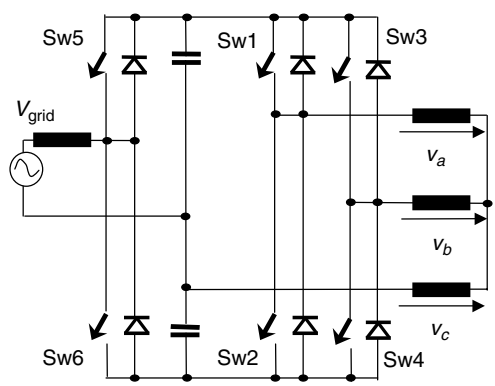

FIGURE 10.2 Reduced component count AC/DC/AC converter.

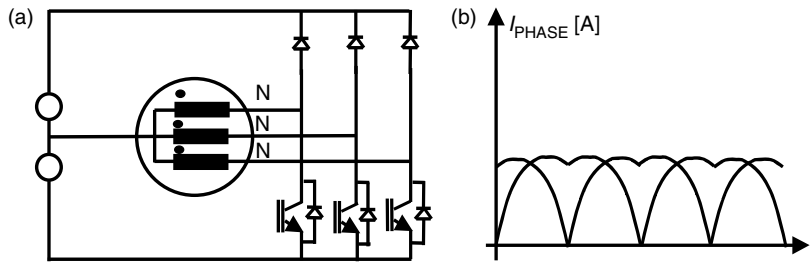

FIGURE 10.3 New DC/AC topology with unidirectional currents: (a) circuit schematics, (b) output phase.

These waveforms can be characterized mathematically by:

$$i_{1d} = I_m[u(\omega t) - u(\omega t - 120)] \sin \omega t + I_m[u(\omega t - 120) - u(\omega t - 240)] \sin(\omega t - 60) \quad (10.1)$$

$$i_{2d} = i_{1d}(\omega t - 120) \quad (10.2)$$

$$i_{3d} = i_{1d}(\omega t - 240) \quad (10.3)$$

One can verify that the difference between two reference currents is a purely sinusoidal wave. For instance: $i_{1-2d} = \mathrm{I}_m \sin \omega t$. It is very important to note that this set of phase currents produces a rotating magnetic field in the machine. In order to demonstrate this, let us first apply the vectorial transform (5.1) to the current waveforms shown in Figure 10.3b. This yields

$$\bar{I} = \frac{2}{3}\left[i_{1d} + \bar{a} i_{2d} + \bar{a}^2 i_{3d}\right] \quad (10.4)$$

where

$$a = \mathrm{e}^{j(2\pi/3)} \quad (10.5)$$

After some calculation:

$$\bar{I} = \frac{1}{\sqrt{3}} I_m \mathrm{e}^{j[\omega t(2\pi/3)]} \quad (10.6)$$

The set of currents from Figure 10.3b generates a rotating magnetic field with constant angular speed and magnitude. A set of currents will be induced in the short-circuited rotor and this will generate another magnetic field. The interaction between the stator and rotor magnetic fields produces a constant electromagnetic torque. The special shape of currents operates the induction machine under unstable conditions and the whole theory of induction machine dynamic model is not applicable here. Analysis should be performed on each interval separately. Stator and

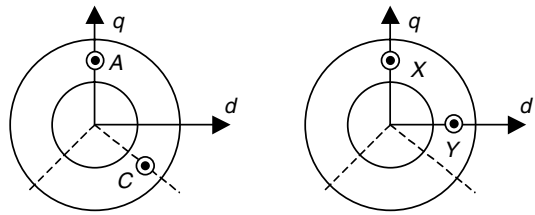

FIGURE 10.4 Transformation of (A, C) to (X, Y) system to prove the operation of the IM drive with the proposed currents.

mutual equivalent inductances yield:

$$\begin{aligned} L_{sX} &= L_{sA} + \frac{1}{2}M_{s(A,C)} = L_s + \frac{1}{2}M_s \\ L_{sY} &= L_{sC} - \frac{1}{2}M_{s(A,C)} = L_s - \frac{1}{2}M_s \\ M_{s(X,Y)} &= \frac{\sqrt{3}}{2}M_{s(A,C)} = \frac{\sqrt{3}}{2}M_s \end{aligned} \tag{10.7}$$

where $L_{sA} = L_{sB} = L_{sC} = L_s$ and $M_{s(A,C)} = M_s$. The resulting voltage equations are similar to traditional dynamic equations for machine modeling except for the values of these inductances. The waveforms of the rotor currents are identical with those carried out for the same drive fed by sinusoidal currents with $I_m/\sqrt{3}$.

A physical explanation of the machine operation is shown in Figure 10.4. Let us consider the time interval with a current passing through the wirings A and C of the stator while the current through the second phase B is zero. An equivalent bi-phase system can be derived for the first $2\pi/3$ rad only if the flux in each wiring produced by the (X, Y) bi-phase system is the same as that produced by the (A, C) system.

Despite the interesting mathematical demonstration of the torque production, this three-phase power converter cannot be practically implemented in the form shown in Figure 10.3a. This is because the currents through the DC mid-point and DC capacitors flow in the same direction and have a tendency to discharge C1 and overcharge C2. In order to prevent this, a special DC/DC converter is proposed in [1,2] to regulate the voltage of the capacitors. This complicates the power stage design.

An alternative solution is proposed in Figure 10.5 [17]. One of the phases is built with a reversed direction and a different number of turns. This solves the problems in the DC bus if that phase current is double the value of each of the other two currents. Unfortunately, this implies a specially built electrical machine, as shown in Figure 10.5.

Using the proposed converter and waveform solution increases losses in the induction machine. A simplified loss estimation is shown here.

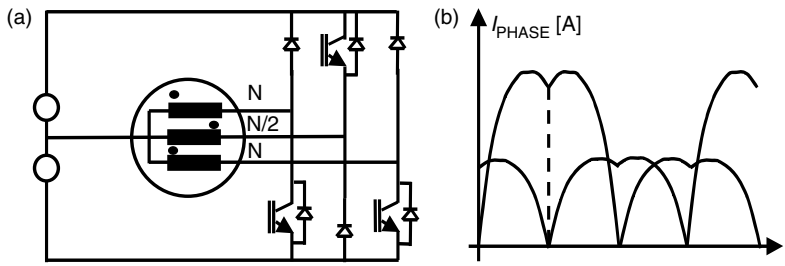

FIGURE 10.5 Implementation of the idea from Figure 10.3.

- Stator copper losses

$$P_{\text{Cus}} = R_s\left[\frac{1}{2\pi}\int_0^{2\pi} i_s^2 \mathrm{d}\omega t\right]$$
$$P_{\text{Cus}} = 0.40\, R_s I_m^2 = 1.2067 R_s\left[i_{\text{ds}}^2 + i_{qs}^2\right] \tag{10.8}$$

  When using the same induction machine (IM) as in a conventional case, an increase of 20.67% stator copper loss occurs.
- Rotor copper losses
  When supplied with the proposed current waveforms, the rotor current's sinusoidal waves and the rotor copper losses can be approximated as identical with the conventional case.
- Iron losses
  A resistor equivalent to the stator iron losses can be included in the simplified IM-equivalent model. This will be passed by a current equal to the difference between the stator current and the current through the magnetizing inductance. For a given torque, the stator losses can be somewhat reduced by a proper adjustment of the magnetic flux.

  Even if these converter solutions are not very practical, they represent good conceptual advances in power converter technologies. Taking into account advanced mathematical theory may lead to new topologies in the future and understanding these advanced converters is a great start in researching emerging conversion approaches.

10.1.2 Direct Converters

Given the cost and size of the passive filter components on the intermediary DC bus, solutions for direct conversion have been sought. First, a very simple but practical solution is presented in [18] and it represents the IGBT equivalent (Figure 10.6b) of a conventional SCR-based AC controller (Figure 10.6a) able to generate a three-phase system of voltages with a constant frequency and variable magnitude.

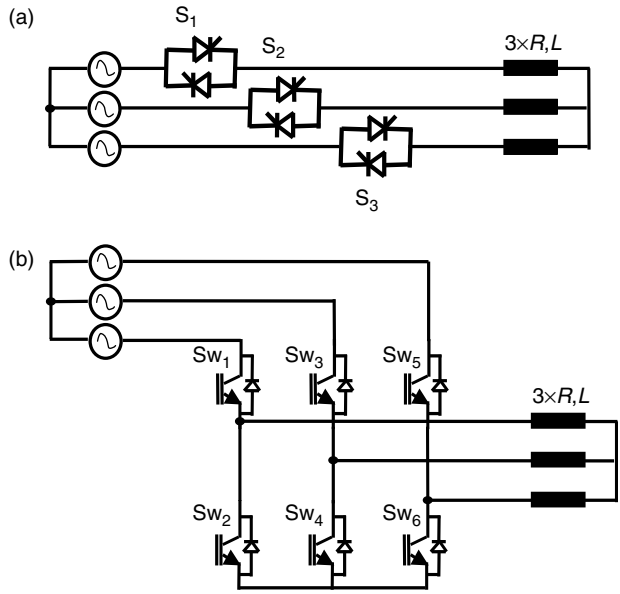

FIGURE 10.6 IGBT-based AC controller.

When high-side IGBTs are controlled, they connect the load to the grid. In contrast, when the low side IGBTs are turned-on, they short the load and separate it from the grid. A train of pulses is created and the root mean square value can be regulated appropriately.

In many motor-drive applications, both frequency and voltage need to be controlled and this can be achieved with different topologies of *matrix converters*. Figure 10.7 shows a three-phase direct AC/AC converter built of three conventional six-switch modules [19–21]. Each module is controlled individually as a boost rectifier producing in output a voltage larger than the magnitude of the grid voltages. This output voltage is controlled with a fixed DC component and a superimposed variable AC component. The load is connected so that it subtracts the DC component and separates the AC components to form a three-phase system.

An important mathematical effort has proven that the motor control and grid interface functions can be separated and controlled independently through the matrix theory [20]:

$$[e] = [H][v_2] \Longrightarrow [v_2] = [H]^{\mathrm{T}}[e] \tag{10.9}$$

$$[H] = [H_f(t)] + [H_\varphi(t)] \tag{10.10}$$

where H_f is the frequency-changer term and H_φ is the power-factor compensation.

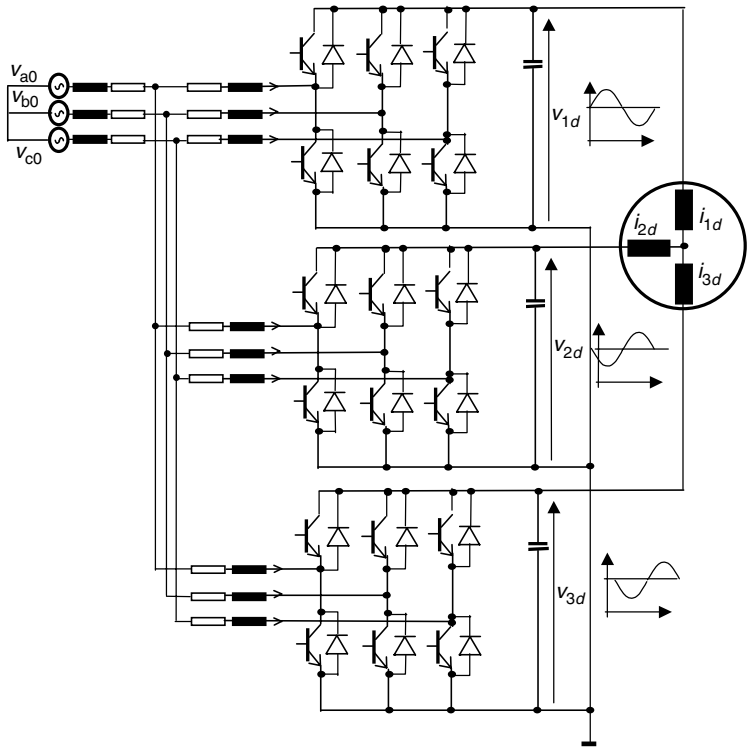

FIGURE 10.7 Schematic diagram of the power stage of the proposed three-phase voltage source matrix converter.

An improved version of control [21] considers a third harmonic injection or the same special shape of voltages from Figure 10.3b in order to increase the maximum available voltage on the load. Both solutions increase the available voltage by 15.6%.

Any of these control solutions has a serious drawback since the voltage required in the power stage during operation is high and the IGBT voltage rating is twice the voltage required by regular three-phase converters.

Another approach to direct AC/AC conversion employs conventional three-phase current source converters, as shown in Figure 10.8, and the appropriate current waveforms, as shown in Figure 10.9 [16]. On the conventional *DC side* of this converter, the current is controlled to show an AC component of desired fundamental frequency superimposed on a DC level. Similar to the converter principle of Figure 10.3a, the current reference waveforms have the shape shown in Figure 10.3b. Each phase current, that is, the DC side current is controlled individually as in the case of a DC magnet power supply [22,23]. Space vector modulation (SVM) control of this topology is introduced in detail in Chapter 13. Due to the individual control of each phase current through a separate power stage that is able to

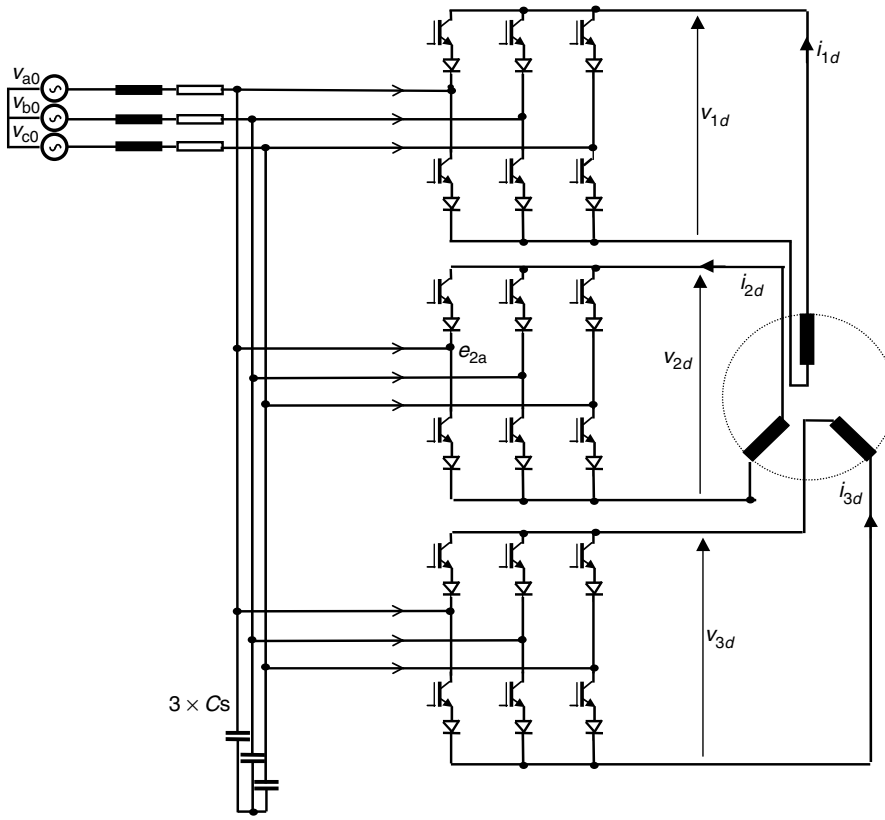

FIGURE 10.8 AC/AC current source matrix converter with unidirectional switches.

also control the input power factor, a special transform function should be used to convert the outputs of the vector control to each individual reference. The mathematical aspects of such function are shown in next section.

The major advantage of this topology relates to a considerable power loss reduction — one out of three converters is always not conducting current. The drawbacks are definitely related to the existence of the DC component in the load currents.

Finally, let us introduce a true three-phase AC/AC matrix converter (Figure 10.10) [27–33]. This topology allows connection of any input phase voltage to any output phase load through a matrix of nine switches. Both scalar and vector control solutions have been extensively studied in the literature. The major drawbacks of this converter are the need for bi-directional switches — special attention in switching current from a switch to another — and an external clamp circuit.

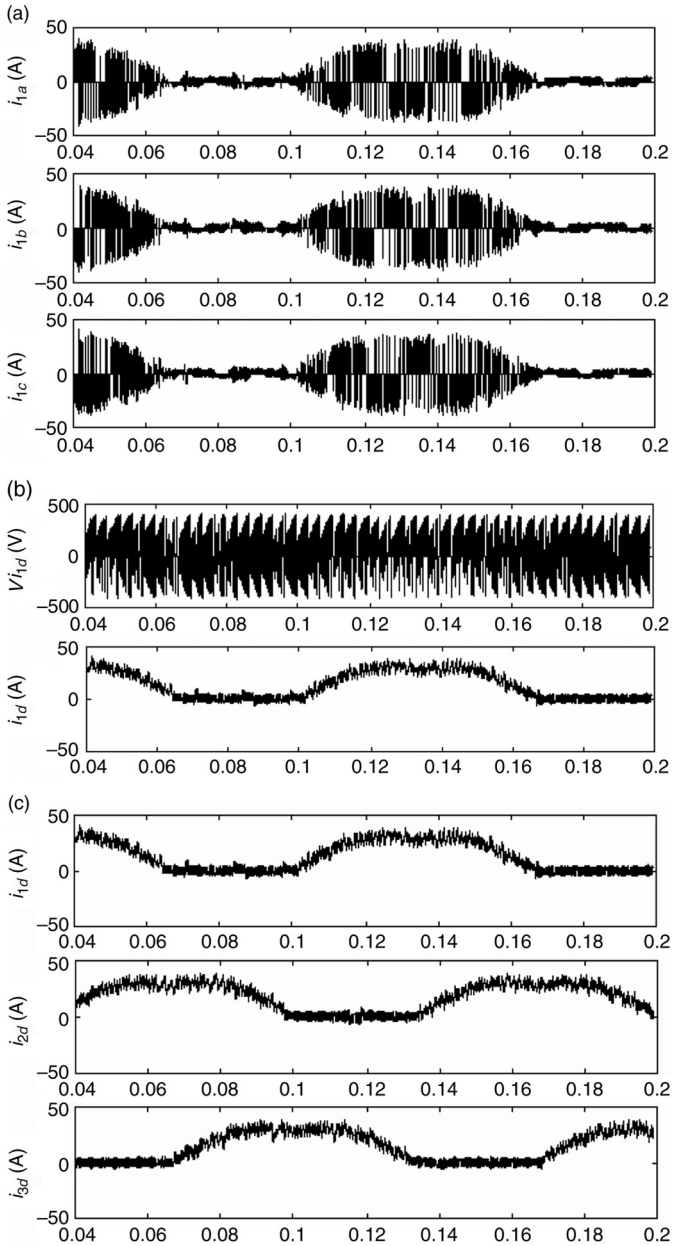

FIGURE 10.9 Waveforms for the first converter plus the command signals ($f_{out} = 10$ Hz, $I_m = 30\,A$, $f_{sw} = 3.6$ kHz, $R_L = 2\Omega$, $L_L = 4$ mH). (a) Input phase currents for one of the converters. (b) Output phase current and output voltage for one converter. (c) Output phase currents for all three converters. (From Neacsu DO, IEEE IECON 1999, Sanjose, CA, USA, Nov.29–Dec.3, 1999. With permission.)

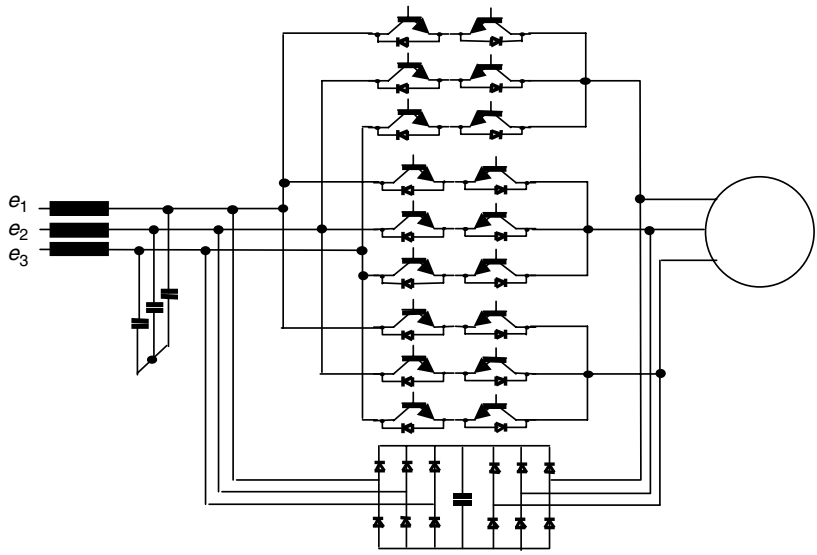

FIGURE 10.10 AC/AC matrix converter.

10.2 GENERALIZED VECTOR TRANSFORM

Some of the previous converters have used a special shape of the phase currents or voltages (Figure 10.3b). This shape of the converter waveform has the interesting property that their difference is always a pure sinusoidal waveform. However, a link between vector control methods and the proposed waveforms is necessary. Conventional vector control methods have orthogonal (d, q) or (x, y) coordinates as outputs.

Let us consider a general set of three voltages [24]:

$$[e] = \begin{bmatrix} e_a \\ e_b \\ e_c \end{bmatrix} \tag{10.11}$$

that needs to be transformed in another set of voltages

$$[v_2] = \begin{bmatrix} v_{1d} \\ v_{2d} \\ v_{3d} \end{bmatrix} \tag{10.12}$$

Usual vector control theory uses the time-invariant environment of d-q-0 frame. We would like now to generalize this transform from a system with frequency ω_1 to a system with frequency ω_2 through an intermediary fixed-gain DC controller. All possible control cases share the same general expression for the direct transfer

function $[H_f]$ [20].

$$[H_f(t)] = [C(\omega_1)]_{3x2}[P]_{2x2}[C(\omega_2)]^T_{3x2} \tag{10.13}$$

where

$$[C(\omega_i)] = [b_1(\omega_i) \quad b_2(\omega_i) \quad b_3(\omega_i)] \tag{10.14}$$

represents a matrix composed of orthonormal base vectors of the input or output three-phase systems and $[P]$ represents a matrix of constant weights p_{ij}. For a three-phase system, the vector space has a dimension of three, and only three terms will always be seen in the matrix defined with base vectors.

Symmetries within a three-phase system contribute to a generalized form of Equation (10.12):

$$[H_f(t)] = \begin{bmatrix} C_{12}(0) & C_{12}\left(\frac{-2\pi}{3}\right) & C_{12}\left(\frac{2\pi}{3}\right) \\ C_{12}\left(\frac{-2\pi}{3}\right) & C_{12}\left(\frac{2\pi}{3}\right) & C_{12}(0) \\ C_{12}\left(\frac{2\pi}{3}\right) & C_{12}(0) & C_{12}\left(\frac{-2\pi}{3}\right) \end{bmatrix} \tag{10.15}$$

A *base* within a vector space consists of a system of vectors B that provides a unique representation of any member V of that vector space as a linear combination of vectors from B. For our 3-dimensional vector space, it yields:

$$\vec{V} = b_1(\omega_j)v_d + b_2(\omega_j)v_q + b_3(\omega_j)v_0 \tag{10.16}$$

or

$$\vec{V} = b_1(\omega_j)v_d + b_2(\omega_j)v_q \tag{10.17}$$

where v_d, v_q, and v_0 are also called coordinates. If the vector space has a finite dimension, then all possible bases have the same number of elements. A base is orthonormalized if all its vectors have unitary magnitude and any two different vectors are orthogonals.

Generally, analysis of three-phase power converters considers the orthonormalized base vectors as:

$$[b_1(\omega_i)]^{\mathrm{T}} = \sqrt{\frac{2}{3}}\left[\cos\omega_i t \ \cos\left[\omega_i t - \frac{2\pi}{3}\right] \ \cos\left[\omega_i t - \frac{4\pi}{3}\right]\right] \tag{10.18}$$

$$[b_2(\omega_i)]^{\mathrm{T}} = \sqrt{\frac{2}{3}}\left[\sin\omega_i t \ \sin\left[\omega_i t - \frac{2\pi}{3}\right] \ \sin\left[\omega_i t - \frac{4\pi}{3}\right]\right] \tag{10.19}$$

$$[b_3(\omega_i)]^{\mathrm{T}} = \sqrt{\frac{1}{3}}[1\ 1\ 1] \tag{10.20}$$

When the zero sequence is omitted, $b_3(\omega_i)$ does not appear in the frequency-changer term.

The intermediary factor, P_f, plays the same role as the turn ratio of the primary to secondary windings of a magnetic transformer. For example, we provide three possible cases here:

(A) Choosing

$$[P]_{2x2} = P_f \begin{bmatrix} 1 & 0 \\ 0 & -1 \end{bmatrix} \tag{10.21}$$

yields

$$C_{12}^{A}(x) = \frac{2}{3} P_f \cos[(\omega_1 + \omega_2)t + x] \tag{10.22}$$

(B) Choosing

$$[P]_{2x2} = P_f \begin{bmatrix} 1 & 0 \\ 0 & 1 \end{bmatrix} \tag{10.23}$$

yields

$$C_{12}^{B}(x) = \frac{2}{3} P_f \cos[(\omega_1 - \omega_2)t + x] \tag{10.24}$$

(C) A general dependency including both type of terms yields

$$C_{12}^{C}(x) = P_f \left\{ \frac{1}{3} \cos[(\omega_1 - \omega_2)t + x] + \frac{1}{3} \cos[(\omega_1 + \omega_2)t + x] \right\} \tag{10.25}$$

Due to the definition of a base in a vector space, a base is not unique and new vector bases can be defined. This demonstrates that the selection of Equation (10.10), and Equation (10.11), Equation (10.12) is not the unique choice for a three-phase system. It opens up a new mathematical tool for working with references not sinusoidal but characterizing uniquely a three-phase system. The resulting waveforms have been also used in discontinuous PWM algorithms.

Figure 10.11 presents two possible waveforms considered as examples for this approach. Furthermore, to simplify the mathematics, the third term corresponding to the homopolar component is neglected in this analysis.

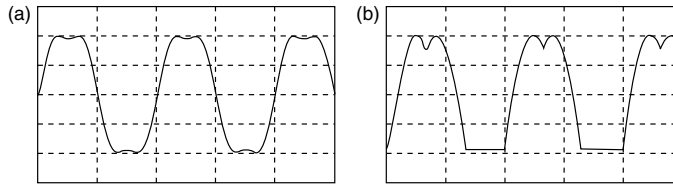

FIGURE 10.11 Different choices of output-side references functions.

The mathematical form of Figure 10.11a yields the following two functions that can be chosen as a base in a vector space.

$$\begin{aligned}[b_1(\omega_2)]^{\mathrm{T}} &= \sqrt{\frac{2}{3}}\left[\cos\omega_2 t + \frac{1}{6}\cos(3\omega_2 t)\ \ \cos\left[\omega_2 t - \frac{2\pi}{3}\right]\right.\\ &\quad \left. + \frac{1}{6}\cos(3\omega_2 t)\ \ \cos\left[\omega_2 t - \frac{4\pi}{3}\right] + \frac{1}{6}\cos(3\omega_2 t)\right]\\ [b_2(\omega_2)]^{\mathrm{T}} &= \sqrt{\frac{2}{3}}\left[\sin\ \omega_2 t + \frac{1}{6}\sin(3\omega_2 t)\ \ \sin\left[\omega_i t - \frac{2\pi}{3}\right]\right.\\ &\quad \left. + \frac{1}{6}\sin(3\omega_2 t)\ \sin\left[\omega_i t - \frac{4\pi}{3}\right] + \frac{1}{6}\sin(3\omega_2 t)\right]\end{aligned} \tag{10.26}$$

Considering the same vector base from Equation (10.12) and Equation (10.13) for $C(\omega_1)$ and the new base functions (Equation (10.20) and Equation (10.21)) on $C(\omega_2)$ yields the next form of the modulating signals.

$$[H_f] = \begin{bmatrix} C_{12}^D(0,0) & C_{12}^D\left(-\frac{2\pi}{3},0\right) & C_{12}^D\left(-\frac{4\pi}{3},0\right) \\ C_{12}^D\left(-\frac{2\pi}{3},\ -\frac{2\pi}{3}\right) & C_{12}^D\left(-\frac{4\pi}{3},\ -\frac{2\pi}{3}\right) & C_{12}^D\left(0,\ -\frac{2\pi}{3}\right) \\ C_{12}^D\left(-\frac{4\pi}{3},\ -\frac{4\pi}{3}\right) & C_{12}^D\left(0,\ -\frac{4\pi}{3}\right) & C_{12}^D\left(-\frac{2\pi}{3},\ -\frac{4\pi}{3}\right) \end{bmatrix} \tag{10.27}$$

where

$$C_{12}^D(x,y) = \frac{2}{3}P_f\left\{\cos[(\omega_1+\omega_2)t + x] + \frac{1}{6}\cos[(\omega_1+3\omega_2)t + y]\right\} \tag{10.28}$$

Analogously, we can consider the base vectors:

$$[b_1(\omega_2)]^{\mathrm{T}} = \sqrt{\frac{2}{3}}\left[f[\omega_2 t]\ f\left[\omega_2 t - \frac{2\pi}{3}\right]\ f\left[\omega_2 t - \frac{4\pi}{3}\right]\right] \tag{10.29}$$

$$[b_2(\omega_2)]^{\mathrm{T}} = \sqrt{\frac{2}{3}}\left[g[\omega_2 t]\ g\left[\omega_2 t - \frac{2\pi}{3}\right]\ g\left[\omega_2 t - \frac{4\pi}{3}\right]\right] \tag{10.30}$$

where $f(\omega_2 t)$ represents the waveform presented in Figure 10.11b and $g(\omega_2 t)$ represents the same waveform with 90° out of phase. It yields:

$$\begin{aligned} f(\omega_2 t) = &\left[u(\omega_2 t) - u\left(\omega_2 t - \frac{2\pi}{3}\right)\right]\cos\omega_2 t \\ &+ \left[u\left(\omega_2 t - \frac{2\pi}{3}\right) - u\left(\omega_2 t - \frac{4\pi}{3}\right)\right]\cos\left(\omega_2 t - \frac{\pi}{3}\right) \end{aligned} \tag{10.31}$$

where $u(x)$ represents the Heaviside function (=0, for $x < 0$ and =1 for $x > 0$).

Finally, denoting:

$$C_{12}^{E}(x, y) = \frac{2}{3} P_f\{\cos(\omega_1 t + x) f(\omega_2 t + y) - \sin(\omega_1 t + x) g(\omega_2 t + y)\} \tag{10.32}$$

yields

$$[H_f] = \begin{bmatrix} C_{12}^{E}(0,0) & C_{12}^{E}\left(0, -\frac{2\pi}{3}\right) & C_{12}^{E}\left(0, -\frac{4\pi}{3}\right) \\ C_{12}^{E}\left(-\frac{2\pi}{3}, 0\right) & C_{12}^{E}\left(-\frac{2\pi}{3}, -\frac{2\pi}{3}\right) & C_{12}^{E}\left(-\frac{2\pi}{3}, -\frac{4\pi}{3}\right) \\ C_{12}^{E}\left(-\frac{4\pi}{3}, 0\right) & C_{12}^{E}\left(-\frac{4\pi}{3}, -\frac{2\pi}{3}\right) & C_{12}^{E}\left(-\frac{2\pi}{3}, -\frac{4\pi}{3}\right) \end{bmatrix} \tag{10.33}$$

10.3 VECTORIAL ANALYSIS OF THE B4 INVERTER

A new inverter topology with reduced count of components is built with two legs of the conventional inverter while the third phase is collected from the midpoint of the DC capacitor bank (Figure 10.1).

Let us first understand how this power converter operates. The third phase is taken from the midpoint of the capacitor bank and its pole voltage (*M-Z*) is always fixed at $V_{\mathrm{DC}}/2$. The phase voltages are constructed through a control on the other two inverter legs. The first consequence is the lack of zero states: there is no way the three pole voltages can be at the same potential during operation. This means that pulse width modulation (PWM) should be developed based on the remaining active vectors (Figure 10.16). A rule of operating a voltage source

TABLE 10.1
Possible Inverter States and Their Appropriate Voltages

Sw1/Sw2	Sw3/Sw4	V_{AZ}	V_{BZ}	V_{AN}	V_{BN}	V_{MN}	V_d (*Re*)	V_q (Im)
1/0	1/0	V_{DC}	V_{DC}	$V_{DC}/6$	$V_{DC}/6$	$-V_{DC}/3$	$\frac{V_{DC}}{6}$	$\frac{V_{DC}}{2\sqrt{3}}$
1/0	0/1	V_{DC}	0	$V_{DC}/2$	$-V_{DC}/2$	0	$\frac{V_{DC}}{2}$	$-\frac{V_{DC}}{2\sqrt{3}}$
0/1	1/0	0	V_{DC}	$-V_{DC}/2$	$V_{DC}/2$	0	$-\frac{V_{DC}}{2}$	$-\frac{V_{DC}}{2\sqrt{3}}$
0/1	0/1	0	0	$-V_{DC}/6$	$-V_{DC}/6$	$V_{DC}/3$	$-\frac{V_{DC}}{6}$	$-\frac{V_{DC}}{2\sqrt{3}}$

three-phase inverter says that we should always have one switch *ON* across each inverter leg. This limits the number of the control states to four as shown in Table 10.1. A set of phase voltages can be generated by a combination of these states.

Phase voltages can be calculated from the pole voltages, as shown in Chapter 3. The appropriate equations are just adapted here to our inverter topology.

$$v_{NZ} = \frac{[v_{AZ} + v_{BZ} + v_{MZ}]}{3} \tag{10.34}$$

$$\begin{cases} v_a = v_{AZ} - \dfrac{[v_{AZ} + v_{BZ} + v_{MZ}]}{3} \\ v_b = v_{BZ} - \dfrac{[v_{AZ} + v_{BZ} + v_{MZ}]}{3} \\ v_c = v_{MZ} - \dfrac{[v_{AZ} + v_{BZ} + v_{MZ}]}{3} \end{cases} \tag{10.35}$$

The first attempts to use this topology have generated PWM with a conventional, reference-triangle, carrier-based method. The reference waveforms have been considered sinusoidal with a 60° phase shift between each other. The pole voltages for the inverter legs can be written as:

$$\begin{cases} v_{AZ} = V\cos(\omega t) + \dfrac{V_{DC}}{2} + f_a(t) \\ v_{BZ} = V\cos\left(\omega t - \dfrac{\pi}{3}\right) + \dfrac{V_{DC}}{2} + f_b(t) \end{cases} \tag{10.36}$$

where f_a and f_b account for the high-frequency components due to switchings. If the load is heavily inductive or a motor drive, it is a good approximation to neglect these harmonics and to consider the effect of the waveforms in fundamental

frequency only. It yields:

$$v_{NZ} = \frac{V_{DC}}{2} + \frac{1}{3}\left[V\cos[\omega t] + V\cos\left(\omega t - \frac{\pi}{3}\right)\right]$$
$$= \frac{V_{DC}}{2} + \frac{1}{3}V\left[2\cos\left[\omega t - \frac{\pi}{6}\right]\cos\left(\frac{\pi}{6}\right)\right] \quad (10.37)$$
$$v_{NZ} = \frac{V_{DC}}{2} + \frac{1}{\sqrt{3}}V\cos\left[\omega t - \frac{\pi}{6}\right] \quad (10.38)$$

and

$$\begin{cases} v_a = \left[\frac{V_{DC}}{2} + V\cos(\omega t)\right] - \left[\frac{V_{DC}}{2} + \frac{1}{\sqrt{3}}V\cos\left[\omega t - \frac{\pi}{6}\right]\right] \\ v_b = \left[\frac{V_{DC}}{2} + V\cos\left(\omega t - \frac{\pi}{3}\right)\right] - \left[\frac{V_{DC}}{2} + \frac{1}{\sqrt{3}}V\cos\left[\omega t - \frac{\pi}{6}\right]\right] \\ v_c = \left[\frac{V_{DC}}{2}\right] - \left[\frac{V_{DC}}{2} + \frac{1}{\sqrt{3}}V\cos\left[\omega t - \frac{\pi}{6}\right]\right] \end{cases} \quad (10.39)$$

$$\begin{cases} v_a = V\left[\cos(\omega t) - \frac{1}{\sqrt{3}}\cos(\omega t)\frac{\sqrt{3}}{2} - \frac{1}{\sqrt{3}}\sin(\omega t)\frac{1}{2}\right] \\ v_b = V\left[\cos\left(\omega t - \frac{\pi}{3}\right) - \frac{1}{\sqrt{3}}\cos\left[\omega t - \frac{\pi}{6}\right]\right] \\ v_c = -\frac{1}{\sqrt{3}}V\cos\left[\omega t - \frac{\pi}{6}\right] \end{cases} \quad (10.40)$$

$$\begin{cases} v_a = \frac{1}{\sqrt{3}}V\left[\frac{\sqrt{3}}{2}\cos(\omega t) - \sin(\omega t)\frac{1}{2}\right] = \frac{1}{\sqrt{3}}V\cos\left(\omega t + \frac{\pi}{6}\right) \\ \quad = \frac{1}{\sqrt{3}}V\sin\left(\omega t + \frac{2\pi}{3}\right) \\ v_b = V\left[\cos(\omega t)\frac{1}{2} + \sin(\omega t)\frac{\sqrt{3}}{2} - \frac{1}{\sqrt{3}}\cos(\omega t)\frac{\sqrt{3}}{2} - \frac{1}{\sqrt{3}}\sin(\omega t)\frac{1}{2}\right] \\ \quad = \frac{1}{\sqrt{3}}V\sin(\omega t) \\ v_c = -\frac{1}{\sqrt{3}}V\cos\left[\omega t - \frac{\pi}{6}\right] = \frac{1}{\sqrt{3}}V\cos\left[\pi - \omega t - \frac{\pi}{6}\right] = \frac{1}{\sqrt{3}}V\sin\left[\omega t - \frac{2\pi}{3}\right] \end{cases} \quad (10.41)$$

In conclusion, this topology can be controlled by two sinusoidal references with 60° out of phase from each other in order to produce a symmetrical three-phase

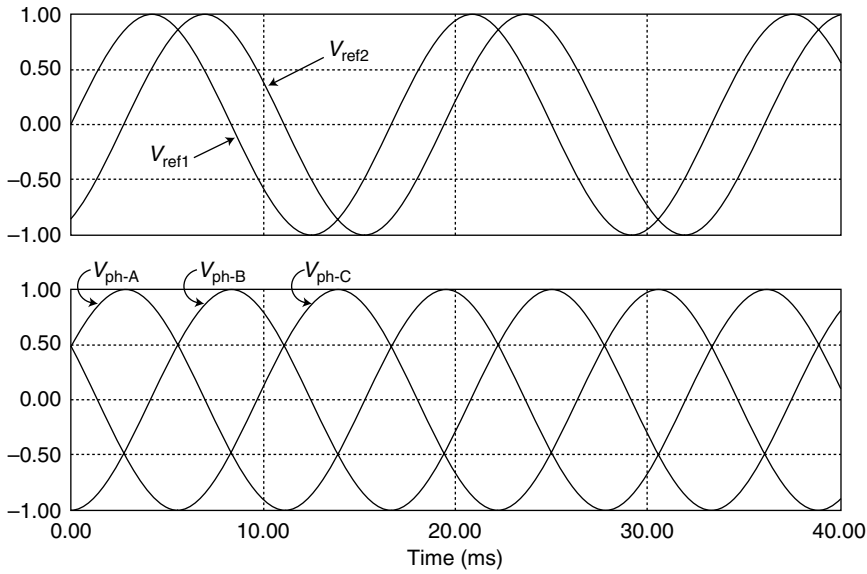

FIGURE 10.12 Phase information for the reference functions and desired fundamental phase voltages on the load (Equation (10.32) and Equation (10.37)).

system. Moreover, these two references should be phase-shifted by 30 degree from the desired first-phase voltage (Figure 10.12).

A similar control can be achieved by vectorial analysis. Let us apply transform relationship (4.1) to the phase voltages shown in Table 10.1. A vector in the complex plane will correspond to each operation mode (Figure 10.11). It is important to note that a different notation of the phase voltages in Figure 10.1 will produce other positions in the complex plane of the active vectors. The vectors shown in the complex plane of Figure 10.13 have magnitudes of $V_{DC}/\sqrt{3}$ and $V_{DC}/3$, respectively.

The generation of a symmetrical three-phase system assumes displacement of the tip of the voltage vector on a circular trajectory. The maximum radius of this circular locus is achieved when the trajectory is tangent to the polygon. It yields:

$$V_{max} = \frac{V_{DC}}{2\sqrt{3}} \Longrightarrow m = \frac{V}{V_{DC}/2\sqrt{3}} \tag{10.42}$$

Let us remember that the maximum voltage obtainable from a conventional six-switch inverter is $(1/\sqrt{3})V_{DC}$ (Equation (5.31)). The B4 inverter needs a double DC voltage in order to produce the same output-phase voltage and this is a serious drawback of this topology. It produces increased voltage stress on the power semiconductor devices and electrical machine. The absolute value of the peak-to-peak ripple on the DC bus capacitor voltage is also increased. Finally, the third-phase current circulates through the DC bank capacitor and this produces

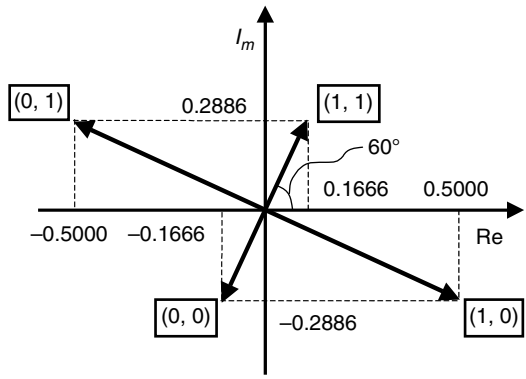

FIGURE 10.13 Vectorial representation of the active vectors corresponding to the B4 inverter.

large variations of the voltage between the two capacitors. This can be corrected with large capacitors.

The two-leg inverter produces asymmetrical phase voltages, as shown in Figure 10.14.

Since one leg circulates currents through the DC capacitor bank, asymmetries of the operation may introduce a third harmonic on the line-to-line voltages. The content of the third harmonic for the leg connected to the capacitor bank is twice as large as the third harmonic in the other two legs as they add up into the first one.

PWM generation takes into account the following constraints due to the asymmetries in operation:

- Decomposition on two adjacent vectors provides the average relationship.
- Because there is no true zero vector, two vectors with opposite directions are considered for equal time intervals to synthesize a zero-voltage state.

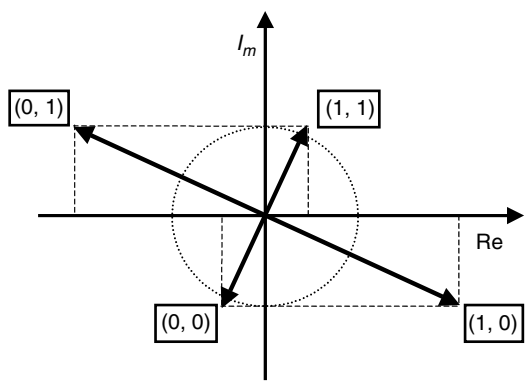

FIGURE 10.14 Typical phase voltages for the converter of Figure 10.1.

- There are always two possibilities for zero-vector generation. It is preferable to use the *short* vectors for this because the *long* vectors produce larger voltage drop on the inductive load and larger ripple.
- In consequence, each vector generation is made with minimum three vectors: two short and one long.
- Several state sequences are possible.

The reduction of the number of switches determines cost reduction as well as conduction loss reduction in the power stage.

10.4 DEFINITION OF PWM ALGORITHMS FOR THE B4 INVERTER

Two vector PWM methods are investigated here.

10.4.1 METHOD 1

The idea of vectorial decomposition on two neighboring vectors is considered for the two-leg inverter. If we consider the desired position of the voltage vector in between V_2 and V_3, the time intervals associated with each state are given by:

$$\begin{aligned} V_s \cos\varphi &= \frac{t_2}{T_s}\lfloor V_2 \rfloor \\ V_s \sin\varphi &= \frac{t_3^1}{T_s}\lfloor V_3 \rfloor \end{aligned} \tag{10.43}$$

$$\begin{cases} t_2 = \dfrac{V_s}{\lfloor V_2 \rfloor} T_s \cos\varphi \\ t_3^1 = \dfrac{V_s}{\lfloor V_3 \rfloor} T_s \sin\varphi \\ t_0 = 2t_3^2 = 2t_1 = T_s - t_2 - t_3^1 \end{cases}$$

$$\Longrightarrow \begin{cases} t_2 = \dfrac{V_s}{\lfloor V_2 \rfloor} T_s \cos\varphi \\ t_1 = \dfrac{1}{2}\left[T_s - \dfrac{V_s}{\lfloor V_2 \rfloor} T_s \cos\varphi - \dfrac{V_s}{\lfloor V_3 \rfloor} T_s \sin\varphi \right] \\ t_3 = \dfrac{V_s}{\lfloor V_3 \rfloor} T_s \sin\varphi + \dfrac{1}{2}\left[T_s - \dfrac{V_s}{\lfloor V_2 \rfloor} T_s \cos\varphi - \dfrac{V_s}{\lfloor V_3 \rfloor} T_s \sin\varphi \right] \end{cases} \tag{10.44}$$

$$\begin{cases} t_2 = \dfrac{V_s}{\lfloor V_2 \rfloor} T_s \cos\varphi \\ t_1 = \dfrac{1}{2}\left[T_s - \dfrac{V_s}{\lfloor V_2 \rfloor} T_s \cos\varphi - \dfrac{V_s}{\lfloor V_3 \rfloor} T_s \sin\varphi \right] \\ t_3 = \dfrac{1}{2}\left[T_s - \dfrac{V_s}{\lfloor V_2 \rfloor} T_s \cos\varphi + \dfrac{V_s}{\lfloor V_3 \rfloor} T_s \sin\varphi \right] \end{cases} \tag{10.45}$$

When vectors V_1-V_3-V_4 are used, these equations are the same with V_4 instead of V_2. Moreover, there are several possibilities for the state sequence:

$$\text{00-10-11-11-10-00} \quad \text{or} \quad \text{11-10-00-00-10-11}$$

As a final verification, the ON-time of the upper switch on the first leg can be calculated as the sum of the time spent on V_2 and V_3:

$$t_a = \frac{1}{2}\left[T_s + \frac{V_s}{\lfloor V_2 \rfloor} T_s \cos\varphi + \frac{V_s}{\lfloor V_3 \rfloor} T_s \sin\varphi\right]$$

$$= \frac{1}{2} T_s \left[1 + \frac{1}{2} m \cos\varphi + \frac{\sqrt{3}}{2} m \sin\varphi\right] \tag{10.46}$$

$$t_a = \frac{1}{2} T_s \left[1 + m \sin\left[\varphi + \frac{\pi}{6}\right]\right] \tag{10.47}$$

The ON-time of the high-side switch of the second leg is t_3:

$$t_b = \frac{1}{2}\left[T_s - \frac{V_s}{\lfloor V_2 \rfloor} T_s \cos\varphi + \frac{V_s}{\lfloor V_3 \rfloor} T_s \sin\varphi\right]$$

$$= \frac{1}{2} T_s \left[1 - \frac{1}{2} m \cos\varphi + \frac{\sqrt{3}}{2} m \sin\varphi\right] \tag{10.48}$$

$$t_a = \frac{1}{2} T_s \left[1 + m \sin\left[\varphi - \frac{\pi}{6}\right]\right] \tag{10.49}$$

These results are similar to the previous carrier-based PWM generation but with a different reference for angular coordinate measurement.

10.4.2 Method 2

The ON-time calculation is achieved in the same way. The difference is in the PWM sequence. The bisectrix of the angles between active vectors splits the complex plane into four sectors. A different state sequence is considered for each such sector:

$$285 < \varphi < 15^\circ : \quad \text{11-10-00-10-11}$$
$$15 < \varphi < 105^\circ : \quad \text{01-11-10-11-01}$$
$$105 < \varphi < 195^\circ : \quad \text{00-01-11-01-00}$$
$$195 < \varphi < 285^\circ : \quad \text{10-00-01-00-10}$$

10.4.3 Comparative Results

Comparative results between these two methods are shown in Table 10.2. It is important to extend the comparison to each phase or line-to-line voltage, as they are different even when controlling the same power converter (Figure 10.15).

TABLE 10.2
Comparison Between Two Vector PWM Methods

		$m = 0.2$	$m = 0.4$	$m = 0.6$	$m = 0.8$	$m = 1.0$
The content on the low harmonics — 3rd harmonic; V_{B-C} and V_{A-C} are half						
Method 1	V_{A-B}	0.1734	0.0191	0.0059	0.0022	0.0015
Method 2	V_{A-B}	0.1752	0.0198	0.0064	0.0025	0.0016
The content on the low harmonics — 5th harmonic						
Method 1	V_{B-C}	0.0542	0.0115	0.0026	0.0023	0.0019
	V_{A-B}	0.0519	0.0109	0.0054	0.0020	0.0015
Method 2	V_{B-C}	0.0535	0.0110	0.0045	0.0018	0.0015
	V_{A-B}	0.0504	0.0102	0.0050	0.0024	0.0015
The content on the low harmonics — 7th harmonic						
Method 1	V_{B-C}	0.0472	0.0111	0.0029	0.0020	0.0016
	V_{A-B}	0.0481	0.0114	0.0032	0.0019	0.0014
Method 2	V_{B-C}	0.0445	0.0096	0.0042	0.0012	0.0010
	V_{A-B}	0.0516	0.0122	0.0038	0.0014	0.0009
The global content in harmonics — HLF calculated with first 500 harmonics						
Method 1	V_{B-C}	9.196	4.207	2.504	1.248	0.955
	V_{A-B}	4.669	2.282	1.526	1.287	1.048
Method 2	V_{B-C}	10.132	4.601	2.680	1.323	1.089
	V_{A-B}	6.613	3.130	1.963	1.063	0.931

Source: Adapted from Blaabjerg F, Freysson S, Hansen HH, and Hansen S, Proceedings of EPE '95, vol. 1, 806–813, 1995, Blaabjerg F, Kragh H, Neacsu DO, and Pedersen JK, EPE '97, vol. 2, pp. 378–385, 1997.

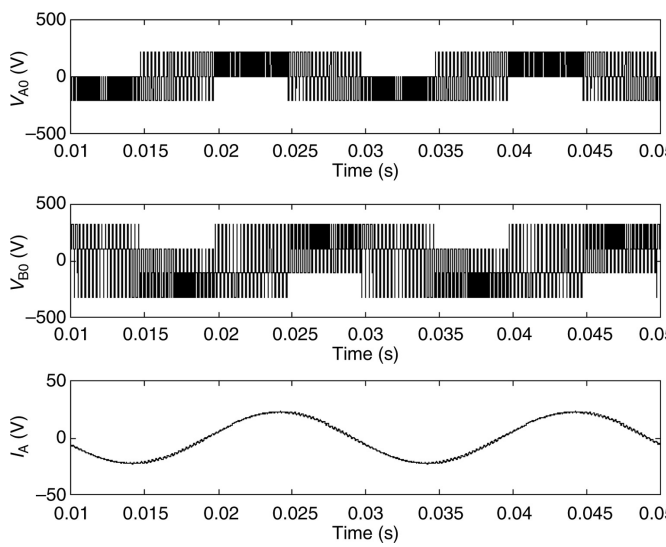

FIGURE 10.15 Maximum modulation index.

10.5 INFLUENCE OF DC VOLTAGE VARIATIONS AND METHOD FOR THEIR COMPENSATION

The DC link voltage is subject to larger ripple than in a conventional six-switch inverter [25,26]. Over and above the expected ripple produced by the rectifier power supply, there is another set of opposite components in each of the DC voltages caused by the phase current circulating through the capacitor bank. These components are stronger depending on the load current level. Moreover, variations of the DC bus voltage have a different influence on each phase voltage in comparison with the six-switch inverter where all phase voltages have been influenced in the same manner.

Chapter 5 has shown that variations of the DC bus voltage can be corrected by a proper adjustment of the SVM algorithm through a feed-forward compensation. The same general concept can be applied to the B4 inverter as well. In this respect, Table 10.1 is rewritten in Table 10.3, based on individual voltages on DC capacitors.

Now, we can rewrite Equation (10.41) by taking into account these values.

$$\begin{cases} t_2 = \dfrac{3V_s}{V_{D1}+V_{D2}} T_s \cos\varphi - \dfrac{V_{D2}-V_{D1}}{V_{D1}+V_{D2}} T_s \\ t_1 = \dfrac{1}{2}\left[T_s - \dfrac{3V_s}{V_{D1}+V_{D2}} T_s \cos\varphi - \dfrac{\sqrt{3}V_s}{V_{D1}+V_{D2}} T_s \sin\varphi \right] \\ t_3 = \dfrac{1}{2}\left[T_s - \dfrac{3V_s}{V_{D1}+V_{D2}} T_s \cos\varphi + \dfrac{\sqrt{3}V_s}{V_{D1}+V_{D2}} T_s \sin\varphi \right] \end{cases} \tag{10.50}$$

The effectiveness of compensation is shown in Figure 10.17.

This example of feed-forward compensation works well before the modulator saturates or tends to go in overmodulation. In other words, the time constants calculated with Equation (10.41) should remain positive at any operation point (Figure 10.18). Let us note ΔV as the absolute value of the ripple within any of the V_1 or V_2 and RV the normalized value of this ripple:

$$RV = \frac{\Delta V}{V_{DC}/2} \tag{10.51}$$

TABLE 10.3
Considering Individual Voltages V_{D1}, V_{D2} on Capacitors

Sw1/Sw2	Sw3/Sw4	V_{AZ}	V_{BZ}	V_{AN}	V_{BN}	V_{MN}
1/0	1/0	$V_{D1}+V_{D2}$	$V_{D1}+V_{D2}$	$V_{D1}/3$	$V_{D1}/3$	$-2V_{D1}/3$
1/0	0/1	$V_{D1}+V_{D2}$	0	$(V_{D1}+V_{D2})/2$	$-(V_{D1}+V_{D2})/2$	$(V_{D2}-V_{D1})/3$
0/1	1/0	0	$V_{D1}+V_{D2}$	$-(V_{D1}+V_{D2})/2$	$(V_{D1}+V_{D2})/2$	$(V_{D2}-V_{D1})/3$
0/1	0/1	0	0	$-V_{D2}/3$	$-V_{D2}/3$	$2V_{D2}/3$

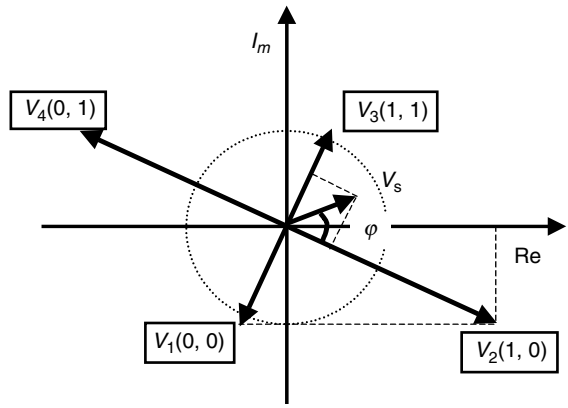

FIGURE 10.16 Vector decomposition.

After some calculation, these limits can be computed as:

$$\begin{cases} RV \leq \dfrac{\sqrt{6}}{4} m \\ RV \leq 1 - m \end{cases} \tag{10.52}$$

Graphical representation of these constraints defines the maximum operational range of this feed-forward method (Figure 10.18).

10.6 TWO-LEG CONVERTER USED IN FEEDING A TWO-PHASE INDUCTION MACHINE

Two-phase IMs are used in several low-power applications around or below 1 kW, especially in automation equipment. They have a reduced starting torque, when

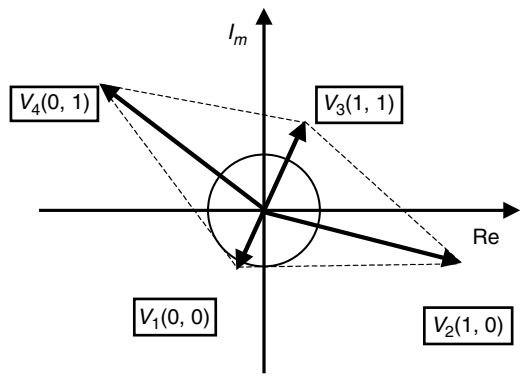

FIGURE 10.17 Deformation of the active vectors due to ripple in the DC bus voltages.

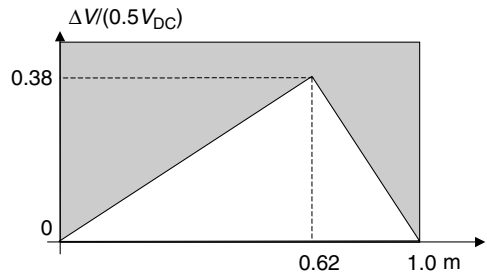

FIGURE 10.18 Maximum correctable ripple by the proposed method.

compared to the DC machines, linear control characteristics, and can be controlled through advanced methods such as field-orientation. The major drawbacks are the reduced efficiency and power factors.

A two-phase inverter with the same power stage as the two-leg inverter (B4) is used for feeding this motor drive (Figure 10.19). This inverter can be supplied from a single-phase diode rectifier suitable to this power level. PWM operation of the IGBT or MOSFET devices building the two-phase inverter ensures variation of both frequency and magnitude of the output voltages. These voltages should be 90° out-of-phase for a proper torque production within the induction motor. Each inverter leg is PWM-operated between voltage levels of $(-V_{DC}/2)$ and $(V_{DC}/2)$ as shown in Figure 10.20.

10.7 CONCLUSION

During the last 20 years of emerging development in power converters, engineers have tried to explore new three-phase solutions for energy conversion. Several topologies are presented in this chapter and they are intended to open new ideas

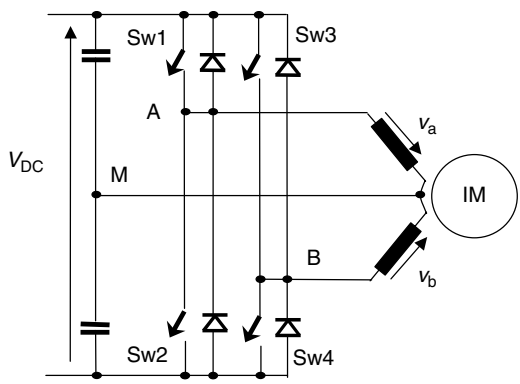

FIGURE 10.19 Two-phase motor drive.

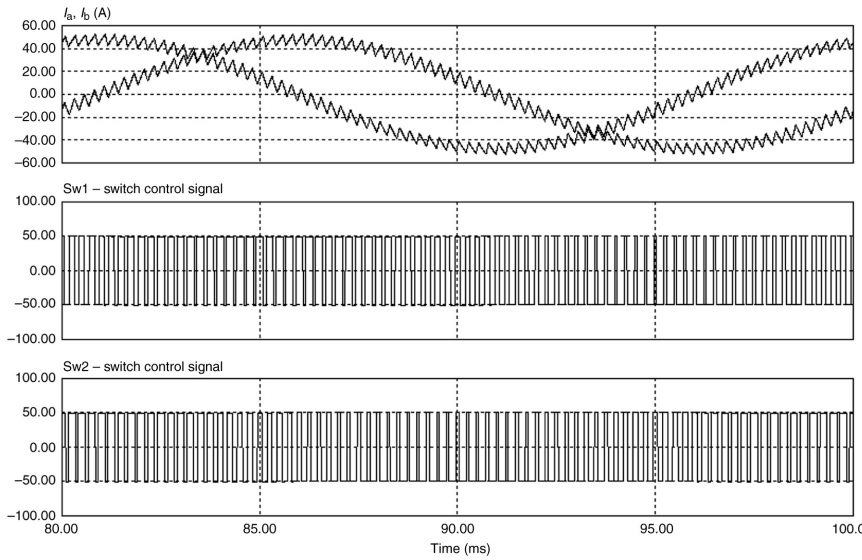

FIGURE 10.20 Significant waveforms at control of a two-phase motor drive with 4 kHz switching frequency. Waveforms shown for $m = 0.5$ and 50 Hz fundamental.

in design of power converters. Each of these solutions has advantages and disadvantages that make them usable in special applications only.

10.8 PROBLEMS

P.10.1 Demonstrate Equation (10.6) by applying $3/2$ transform to Equation (10.1), Equation (10.2), and Equation (10.3).

P.10.2 What are the voltages across and the currents through the IGBTs of Figure 10.6 during the two operation modes?

P.10.3 The converter of Figure 10.7 needs IGBTs rated twice the voltage needed in a conventional three-phase converter. What is the comparative current rating?

P.10.4 What are the voltages across and the currents through the IGBTs of Figure 10.8 during different operation modes?

P.10.5 Demonstrate Equation (10.38).

REFERENCES

1. Covic GA, Peters GL, and Boys JT, An Improved Single Phase to Three Phase Converter for Low Cost AC Motor Drives, Proceedings of PEDS'95, Singapore, vol. 1, pp. 549–554, 1995.
2. Eastham JF, Daniels AR, and Lipcynski RT, A novel power inverter configuration, *IEEE IAS* 2: 748–751, 1980.

3. van Der Broeck HW and Van Wyk JD, A comparative investigation of a three-phase induction machine drive with a component minimized voltage-fed inverter under different control options, *IEEE Trans.* IA, 20: 309–320, 1984.
4. van der Broeck HW and Skudelny HC, Analytical analysis of the harmonic effects of a PWM AC drive, AC, *IEEE Trans. PE*, 3(2): 216–223, 1988.
5. Blaabjerg F, Freysson S, Hansen HH, and Hansen S, A new optimized space vector modulation strategy for a component minimized voltage source inverter, *IEEE APEC*, 2: 577–585, 1995.
6. Blaabjerg F, Freysson S, Hansen HH, and Hansen S, Comparison of a Space-Vector Modulation Strategy for a Three-Phase Standard and a Component Minimized Voltage Source Inverter. Proceedings of EPE'95, vol. 1, 806–813, 1995.
7. Blaabjerg F, Neacsu DO, and Pedersen JK, Adaptive SVM to compensate DC Link voltage ripple for component minimized voltage source inverters, *IEEE PESC*, 1: 580–589, 1997.
8. Blaabjerg F, Kragh H, Neacsu DO, and Pedersen JK, Comparison of Modulation Strategies for B4-Inverter. EPE'97, vol. 2, pp. 378–385, 1997.
9. Jacobina CB, da Silva ERC, Lima AMN, and Ribeiro RLA, Vector and scalar control of a four switch three phase inverter, *IEEE IAS*, 3: 2422–2429, 1995.
10. Kim GT and Lipo TA, VSI-PWM inverter/rectifier system with a reduced switch count, IEEE IAS Thirteenth Annual Meeting, Orlando, FL, USA, vol. 3, pp. 2327–2332, 8–12 October, 1995.
11. Ribeiro RLA, Jacobina CB, da Silva ERC, and Lima AMN, AC/AC converter with four switch three-phase structures, *IEEE PESC*, 1: 134–139, 1996.
12. Alexa D, Static frequency converter with double-branch inverter for supplying three-phase asynchronous motors, *EPE J.*, 5(1): 23–26, 1995.
13. Enjeti P and Rahman A, A new single-phase to three-phase converter with active input current sharing for low cost AC motor drives, IEEE Transactions on Industry Applications, 29(4): pp. 806–813, July–August 1993.
14. Pan CT, Chen TC, Hong YH, and Hung CM, A new DC link converter for induction motor drives, *IEEE Trans. EC*, 10(1): 71–77, 1995.
15. Neacsu DO, Gatlan C, and Gatlan L, A Three-Phase Sinusoidal Current Rectifier with three Unidirectional Switches and Input Transformer. EPE'99, September 2–4, 1999.
16. Neacsu DO, Current-controlled AC/AC voltage source matrix converter for open-winding induction machine drives, Proceedingss of the 25ths Annual Conference of the IEEE Industrial Electronics Society, San Jose, CA, USA, vol. 2, pp. 921–926, 29 November– 3 December, 1999.
17. Welchko B and Lipo TA, A novel variable frequency three-phase induction motor drive system using only three-switches, *IEEE Trans. IA*, 37(6): 1739–1745, 2001.
18. Ziogas PD, Vicenti D, and Joos G, A practical PWM AC controller topology, Conference Record of the 1992 IEEE IAS Tenth Annual Meeting, IEEE-IAS, Houston, TX, USA, pp. 880–887, 3–5 October, 1992.
19. Kazerani M and Ooi BT, Direct AC–AC matrix converter based on three-phase voltage source converter modules, *IEEE IECON*, vol. 2, 812–817, 1993.
20. Ooi BT and Kazerani M, Application of dyadic matrix converter theory in conceptual design of dual field vector and displacement factor controls, *IEEE IAS*, 903–910, 1994.
21. Neacsu DO, Alistar A, and Kazerani M, Insightful Analysis of Carrier PWM Algorithms for Direct AC–AC Matrix Converters Based on Voltage-Source Converter Modules. IEEE IAS 2002, October 13–19, 2002.

22. Enjeti P and Xie B, A new real time space vector PWM strategy for high performance converters, Conference Record of the 1992 IEEE IAS, Tenth Annual Meeting, IEEE-IAS, Houston, TX, USA, pp. 1018–1024, 3–5 October, 1992.
23. Pan CT and Chen TC, Modeling and analysis of a three phase PWM AC–DC converter without current sensor, *IEE Proc. B*, 140(3): 201–208, 1993.
24. Halmos P, *Finite Dimensional Vector Spaces*, Springer-Verlag, New York, 1986.
25. Lee JY and Sun YY, Adaptive harmonic control in PWM inverters with fluctuating input voltage, *IEEE Trans. IE*, 33(1): 92–98, 1986.
26. Enjeti P and Shireen W, A new technique to reject DC link voltage ripple for inverters operating on programmed PWM waveforms, *IEEE Trans. PE*, 7(1): 171–179, 1992.
27. Venturini M, A new sine wave in, sine wave out, conversion technique eliminates reactive elements, in Proc. Powercon 7, San Diego, CA, pp. E3:1–E3:15, 1980.
28. Venturini M and Alesina A, The generalized transformer: A new bidirectional sinusoidal waveform frequency converter with continuously adjustable input power factor, in IEEE PESC Conf. Rec., 1980, pp. 242–252.
29. Alesina A and Venturini M, Analysis and design of optimum amplitude nine-switch direct AC-AC converters, *IEEE Trans. Power Electron*., 4(1): 101, 1989.
30. Jun Oyama, Tsuyoshi Higutbi, Eiji Yamada, Takashi Koga, and Llpo T, New control strategy for matrix converter, IEEE PESC Confernce Record, 1989, pp. 360–367.
31. Ishiguro A, Furuhashi T, and Okuma S, A novel control method for forced commutated cycloconverters using instantaneous vahres of input tine-to-tine voltages, IEEE Trans. on Power Electron., 38(3): 1991.
32. Huber L and Borojecvic D, "Space vector modulated three-phase to three-phase matrix converter with input power factor correction," *IEEE Trans. on Industry Applications*, 31(6): 1234–1245, November, 1995.
33. Klumpner C, Nielsen P, Boldea I, and Blaabjerg F, "New matrix convertor-motor (MCM) for industry application," *IEEE Transactions on Industrial Electronics*, 49(2): 325–335, 2002.